The effect of ageing process on three-point bending strength and permeability of 3D printed sand molds

Saptarshee Mitra, Antonio Rodríguez de Castro, Mohamed El Mansori

The Effect of Ageing Process on Three-Point Bending Strength and Permeability of 3D Printed sand molds

Saptarshee MITRA[1*], Antonio RODRÍGUEZ DE CASTRO[2], Mohamed EL MANSORI[1]

[1]*Laboratoire MSMP – EA7351, Arts et Métiers ParisTech, 2 Cours des Arts et Métiers, 13617Aix-en-Provence, France*

[2]*Laboratoire MSMP – EA7350, Arts et Métiers ParisTech, Rue Saint Dominique, 51006 Châlons-en-Champagne, France*

ABSTRACT

The objective of this paper was to investigate the effects of curing parameters (i.e., temperature and time), on the permeability and mechanical strength of the printed molds. Several sets of samples were hence produced with a state-of-the-art 3D printer using well-characterized silica sand and furan resin binder. Then, experiments were performed in which the evolution over time of the three-point bending (3PB) strength and permeability of the samples were monitored at three different curing temperatures. From these measurements, both the individual and combined effects of curing temperature and time on the functionality of the 3D printed molds were assessed. Moreover, Loss-On-Ignition (LOI) tests were also performed in order to relate the loss of binder mass to the variation in permeability and mechanical strength of the samples. The results showed that the printed molds can be stored at room temperature for a long time before being used, roughly preserving the initial properties. No significant change in 3PB strength was observed when curing at 100ºC. In contrast, the permeability was shown to decrease with increasing curing temperature.

Keywords: Additive manufacturing; 3D Printing; Ageing; Mold characterization; Sand casting; Permeability; Three-point bending strength.

[*] Corresponding author : saptarshee.mitra@ensam.eu

I. INTRODUCTION

Additive Manufacturing (AM), commonly referred to as Three-Dimensional Printing (3DP) was invented at MIT as a rapid prototyping technique to build three-dimensional parts directly from computer design model in layers [1–4]. In 3DP processes, a sliced 3D CAD design is used as input to print up a mold layer upon layer by binding granular material. AM can be defined as the process of joining particles to form an object layer upon layer from 3D design data, in contrast to subtractive manufacturing. Nowadays, 3DP has become the standard method for the production of molds and cores in casting industry as recently reviewed [5], with applications in various areas, such as aircraft, automobiles, and medical. The process of rapid prototyping has been widely accepted due to its significant potential to reduce the cost of manufacturing highly complex components [6–8]. Indeed, amongst all the rapid tooling and manufacturing processes, 3DP makes the most sense for quick integration into existing industries as it can produce high quality and complex sand molds adapted to casting applications within a short time frame [9]. Furthermore, the use of binder jetting technique to produce optimized part designs results in reductions in weight up to 33% as compared to traditional sand mold making process or even any other 3D printing technique [10].

The layer-based 3DP technology produces porous parts by binding individual particles, which generates permeable molds as required for metal casting. In the case of casting sand molds, ceramics are used as particle materials to provide refractoriness, and a liquid binder is used to ensure cohesion between particles by forming capillary bridges between the sand grains, as schematically shown in Fig.1. In particular, a capillary pressure is generated by the curvature of the liquid interface causing attraction between grains and high stiffness of the 3D printed parts. This generates a network of sand grains connected by resin bridges, which is suitable for printing complex casting sand molds. A detailed Scanning Electron Microscope (SEM) analysis of cross-linked resin bridges between sand particles was provided by researchers [11].

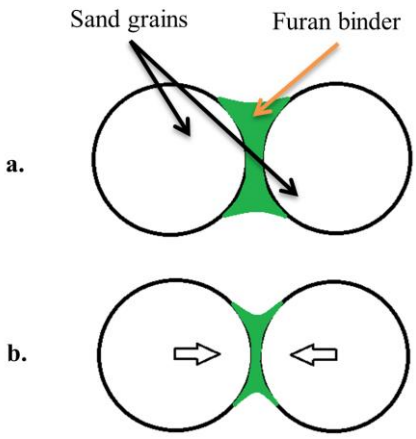

Fig.1 Schematic representation of, **(a)** particle binder bonding and resin bridge in 3D printed sand molds, **(b)** tighly packed particles

The interstices between the grains of sand in the 3D printed parts permit the evacuation of air during the filling of the mold as well as the flow of the gases generated during filling and solidification of the alloy. These gases are evacuated more or less rapidly depending on the permeability of the sand [12, 13]. Researchers have studied the gas emissions from mold and core sand binders, where the thermal degradation of binders was measured by collecting off gasses in specially designed ventilation hood at a constant flow rate [13]. Also a numerical model was developed to estimate the potential out-gassing of the furan bonded silica molds and cores [12]. In this respect, liquid binder blocks gas flow through the sand, resulting in slow filling of the mold cavity and more gas being trapped during pouring of the alloy. Therefore, the permeability of the mold must be high enough to accelerate filling and minimize casting defects. However, excessively high permeability values obtained by using coarse grains of sand may also lead to metal penetration defects due to large inter-sand grain spacing, so a compromise between both effects should be found.

It should be noted that molds with excessively high levels of mechanical strength may give rise to hot tearing and high residual stresses resulting in casting defects [14, 15]. So casting sand molds should exhibit convenient mechanical strength to be handled during casting operations without deteriorating. Researchers have also investigated the surface roughness of the parts casted with 3DP molds, and showed that the surface roughness is dependent on the

temperature of the molten metal and solid fraction at the instant of contact [16]. The flexural strength of the mold is a function of the grain size, binder content present in the mold and sand compaction [17, 18]. The effect of molding parameters (sand grain size, binder percentage and curing time) on chemically bonded sand mold mechanical properties (compression strength, shear strength and core hardness) were studied and was reported that their mechanical properties were found to increase with an increase in binder content and curing time [11]. It was also reported that high amounts of binder lead to more tensile and flexural strength but would affect the dimensional accuracy and surface uniformity of molds [19]. The evidence of evaporation of solvent and shortening of resin bridges were also provided using SEM analysis. Indeed, the binder evaporates during filling and cooling of the mold and a chemical reaction may occur when the liquid binder gets into contact with the binder, releasing gases. High amounts of binder lead to more flexural strength of the sand and shrinkage due to hardening and shortening of resin bridges, but generates excessive gas during casting operations [20–22]. This may result in poor quality of the casting part [21] and incomplete filling of the mold [23].

Organic furan binders are commonly used in foundries for 3DP of sand molds to cast light alloys [14, 15, 21, 23–26]. The impact of temperature on furan resin and binder structure was studied using spectrometer and was reported that the furan resin bonded sand is advantageous in making molds and cores of complex shape with precise dimensions [27]. Also, the curing mechanism of furfuryl alcohol and urea-formaldehyde furan resin were investigated using infrared spectroscopy (IR) technique and was reported that the main advantage of furan binder is that it cures at room temperature and possesses good mechanical strength [24]. Evidence was provided in the formation of three-dimensional structure due to dehydration polycondensation of –OH and addition reaction of C=C resulting in high mold strength. The furan binder condensation reaction produces water, which tends to slow down the rate of curing and hence affects the 3-point bending strength and permeability [28, 29]. Also, more water is evaporated from the mold when the ageing time of the 3DP part is increased.

The effects of ageing parameters on the mechanical properties (strength and permeability) of the mold were previously studied using the ZCast 501 powder and Zb56 resin binder system of the Z Corporation [20]. In this work, the temperature was varied from 150° to 250°C with a

curing time variation of 4-8 h. Others used cylindrical Z-cast samples to optimize the temperature and time for maximum compressive strength, finding that the effect of ageing time on the strength was negligible [30]. Also, researchers optimized the ageing cycle by considering the casting defects due to off-gassing of volatile binder components, showing that the optimum ageing cycle was at 316°C for 1 hour. Moreover, this optimized curing cycle also provided molds with convenient mechanical strength. However, the effects of curing temperature were not investigated and the range of curing times considered was limited to several hours. In particular, higher curing temperatures are known to accelerate the curing process [27].

The objective of the present work is to study the effects of curing parameters, i.e. curing time and temperature, on the strength and permeability of the 3DP sand molds. To do so, the ageing mechanisms were experimentally investigated using a set of 3DP samples produced with chemically-bonded sand as the ones used in casting applications. The evolution of the permeability and the three-point bending strength of the samples was monitored over a long time (up to 45 days) and related to the amount of binder present in the 3DP mold. The initial amount of binder was characterized by means of Loss on ignition (LOI) experiments, the mechanical strength was measured through standard 3-point bending tests and the permeability was determined by measuring the air flow rate through the samples at a given pressure. The experimental results extended our understanding of the ageing mechanisms in 3DP sand molds and provided rigorous criteria for the choice of the ageing parameters.

II. THEORETICAL BACKGROUND

A porous medium is a type of matter composed of a solid matrix containing void spaces that can be discretized as individual pores. Gas or fluids can flow through the connected porosity of these materials, e.g. air through chemically-bonded casting sand, or be contained within the interstices of the solid matrix, e.g. liquid binder. Expendable molds used in casting processes are commonly made from quasi-spherical silica grains which are packed constituting a porous medium. Quartz is the only stable form of silica polymorph at normal ambient conditions, and

the density value of α-Quartz (Silica) is known to be 2648 kgm^{-3}. Therefore, the overall density of a given pack of quartz grains can be calculated by multiplying the density value of quartz by (1 - ε), where ε is the global porosity of the type of packing:

- Simple cubic packing = $\pi/6 \times 2648$ kg m^{-3} = 1376.96 kg m^{-3}
- Centred cubic packing = $\pi\sqrt{3}/8 \times 2648$ kg m^{-3} = 1800.64 kg m^{-3}
- Face-Centred Cubic = $\pi/ 3\sqrt{2} \times 2648$ kg m^{-3} = 1959.52 kg m^{-3}

It is reminded here that the theoretical maximum porosity for a simple cubic packing of uniform sand grain size is ε = (1- π/6) and is obtained with a simple cubic packing.

The mechanical properties of sand packs mainly depend on the adhesion ability of adjacent sand particles sticking to each other and also on the cohesion properties of the binder. The binder liquid should exhibit convenient shear viscosity to fill the interstices without flowing down by gravity and the surface tension should be smaller than that of the water.

Permeability can be defined as the ability of gases to flow through a porous media driven by a pressure gradient and depends on the particle shape, the particle size distribution of the solids forming the bed and the packing structure (i.e. bed bulk porosity). In casting, the pressure gradient is generated by the melt-head pressure during filling of the mold with the liquid alloy and the shrinkage of the solidified alloy during cooling. Darcy's equation [31] is commonly used to predict creeping laminar flow through a porous medium of permeability k when the inertial effects are negligible. Using this equation, the flow rate Q of a gas with shear viscosity μ driven by a pressure gradient of ΔP through a core material of cross sectional area A and length L can be calculated as:

$$Q = \frac{kA}{\mu L}\Delta P \tag{1}$$

For the simplest case in which the packing material is formed by mono-sized spheres, Kozeny–Carman equation can be used to calculate permeability by assuming a bundle of cylindrical capillaries model:

$$k = \frac{\varepsilon_{bed}^3 \, d_s^2}{180(1-\varepsilon_{bed})^2} \quad (2)$$

where ε_{bed} is the average bulk porosity of the packed bed, d_s is the diameter of the spheres and 180 the Kozeny–Carman pre-factor.

Three-point bending (3PB) tests are commonly used to assess the mechanical properties of brittle materials, which are difficult to test these materials with standard tensile tests. 3PB tests are relatively easy to set up and interpret and are usually conducted on a rectangular bar of the tested material, which is placed over two roller supports while the load is applied via a third roller typically mounted halfway between the supports. The bending stress calculation from the measured load is given by Eq. (3):

$$\sigma = F \times \frac{3l}{2bd^2} \quad (3)$$

where F is the load at the middle section of the bar, l is the length between the support span, b is the width of test bar and d is the thickness of the tested sample.

The present work experimentally investigates the individual and combined effect of ageing and mass loss on the bending strength and permeability of 3DP sand molds.

III. EXPERIMENTAL SETUP

Materials

The typical compositions of resin bonded sands used to produce casting molds and cores are 93-99% silica and 1-3% binder [32]. Silica sand is one of the most abundant materials on the earth's crust, and the commercially available standard sizes for mold production are 140 µm, 190 µm and 250 µm [33].

In the particular case of the present experiments, the components of the molding sand were quartz silica sand and a furfuryl-alcohol-based binder of density (1.1-1.2) g/cm³ [34, 35] also known as furan resin binder. The morphology of the silica sand particles (SiO2 99.1%) presents a regular spherical shape, average particle size of 140 µm and a standard deviation of 20 µm. corresponding to American Foundry Society (AFS) size number of 97 [34]. The furan binder was a mixture of furfuryl alcohol (70-90 wt%), bisphenol A (5-15 wt%), resorcinol (1-10 wt%) and 3-aminopropyltriethoxysilane (0.1-0.2 wt%) [35]. [35].

The purpose of adding binder and catalyst [29, 36] is to give additional cohesion and strength to the powder, to ease the mold to retain its shape under a change in pressure, thermal expansion, and erosion when in contact with liquid metal. A Furan Binder (FNB) made up of an acid catalyst, furfuryl alcohol resin, urea and formaldehyde was used in the present experiments. Toluolsulfonic acid was used as catalyst to accelerate the generation a 3-dimensional chain network through acid-hardening reaction and polycondensation when added to the furan resin, leading to hardening of the binder. The FNB's condensation reaction produces water, which tends to slow down the cure rate (dehydration) [36].

Printing procedure and parameters

The specimens were first designed using Catia V5 and then converted into .stl file format. Each sample was engraved with the specimen number to ease identification. The .stl file was transferred to NetFabb software, which is a connected software for additive manufacturing and design. The Schematic design of a Job-Box in NetFabb^{TM} is provided in Fig.2.

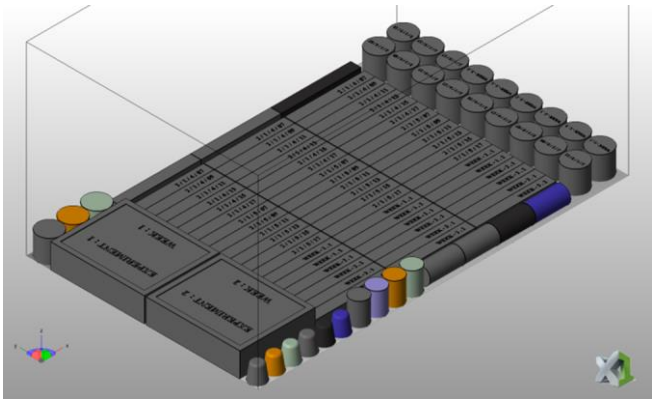

Fig.2 Schematic design of a Job-Box (NetFabb)

For the present work, the specimens were 3D-printed by means of the ExOne S-Print Furan [39] machine shown in Fig.3, with a job box size of 800 × 500 × 400 mm^3. The printing process started by mixing sulfonic acid catalyst with 8 kg of silica sand particles inside a mixing chamber. Sand layers of 280-µm (i.e. 2 time size sand particle) thickness were spread successively over the build platform (X-Y plane) and then a compacting force was applied over the sand bed by means of a re-coater. Then, the print head nozzle injected the liquid binding adhesive (furfuryl alcohol binder) on top of the sand layers to bind them. As the binder droplets were injected over the layer of acid activated sand bed, this facilitates the formation a thin coating of furan binder on each individual sand grain. The surface of this binder coated sand grains crosslink with each other, forming a nearly cylindrical binder bridge between the sand particles. This bridge is generated by capillarity immediately after application of the binder and the corresponding strengthening mechanism occurs progressively over time. This makes the sand particles bond closer, experiencing surface tension and forming a strong binder-particle bridge. The 3DP samples were formed where the sand powder bounds to the liquid binding agent and unbounded sand remained surrounding the printed part. The entire process continues until the last slice of the sample was printed.

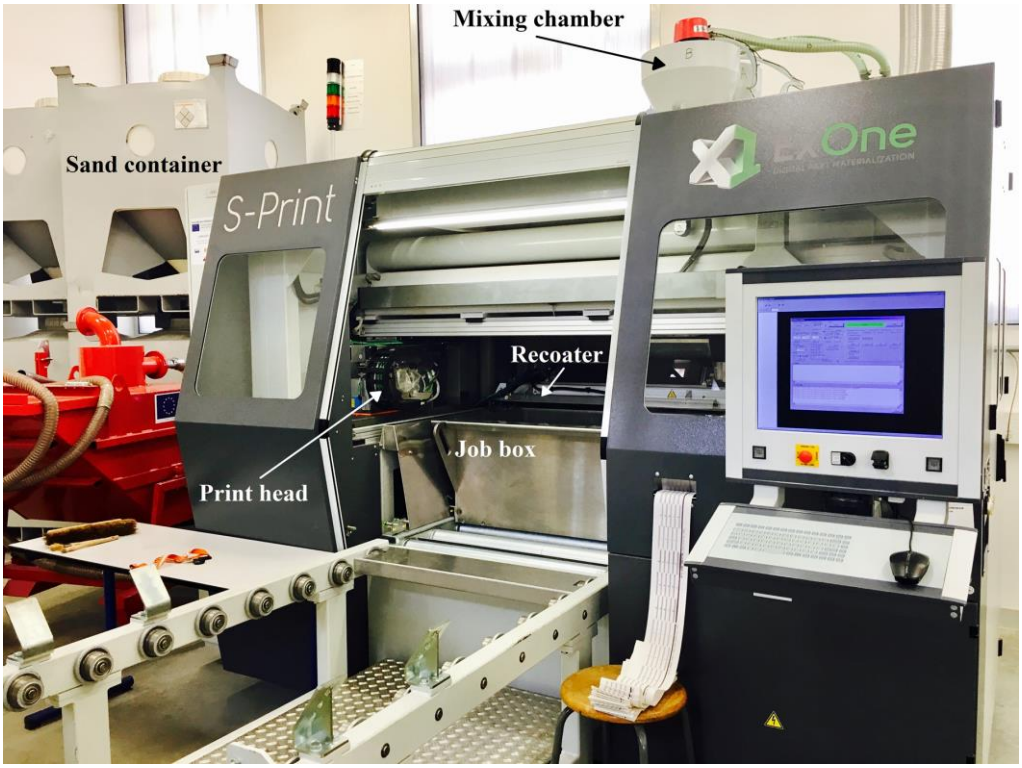

Fig.3 3D sand printer used in the present experiments

The printed specimens were then taken out of the job box and de-powdered. During the process of de-powdering, the unbounded sand particles were removed using soft brushes and air-blown. The printing process parameters are listed in Table 1 and were chosen in agreement with preceding literature [40, 41]. It is noted that spreading of sand at high speed by the recoater leads to non-uniform compaction of the sand bed and consequently lower packing density due to high porosity. In contrast, low values of recoating speed lead to high sand density, inducing greater flexural strength [17]. For this reason, 0.182 m/s (14% of the maximum achievable speed by the recoater-Sprint ExOne) were chosen. The print head voltage determines the volume of each furan droplet with the voltage set and was kept constant. Also, the printing resolution (furan drop spacing) was kept constant. The unbounded sand grains do not provide a good support for parts built higher up in the build volume, which may result in sinking of the specimens into the excess powder during compaction [42–44]. Therefore, the specimens were always printed over a thick sand layer of 1.4mm in the bottom of the job-box in order to neglect the sink issue and sub-layer displacements [42]. It is highlighted that quasi-identical binder contents were expected for all printed samples as the printing parameters were kept constant.

The specimens were printed inside a room with standard room conditions, at a temperature of 25 ± 1 °C and relative humidity of 40 ± 10%. 6 Job-Boxes (Fig 2) were printed. A total of 465 samples were printed: 324 bars with square section (172 x 22.4x 22.4 mm^3) for 3PB strength tests, 126 cylindrical specimens (diameter = 50mm, height = 50mm) for gas permeability tests, 9 bars with square section (172 x 22.4x 22.4 mm^3) for mass loss test, 3 similar rectangular bars for sand 3DP mold porosity test, and 3 cubic specimens for loss on ignition (LOI) tests. In order to estimate the uncertainty of the measurements, 3 specimens were measured at each curing time for the 3PB test and 1 cylindrical specimen was measured 3 times for each permeability test. The initial dimensions of the 3D printed parts (bars) were measured using a Vernier caliper, with length, breadth and height of 22.2 ± 0.02 mm, 22.3 ± 0.02 mm and 171.8 ± 0.08 mm, respectively (95% confidence interval). The initial 3PB strength and permeability of the 3DP specimens was measured after printing of the samples, obtaining 1.75 ± 0.5 MPa and 60 ± 7 GP, respectively. The procedures used to measure the mechanical strengths and the permeability of the samples are presented in sections 3.6 and 3.7, respectively.

Table.1 Printing process parameters used with ExOne S-Print furan machine

Ageing process

As mentioned in section 2, the higher the amount of binder in a mold, the greater is its mechanical strength. However, higher binder contents are known to result in off-gassing and incomplete filling that may hinder the filling of the sand mold cavity [21, 25, 45]. Therefore, it is necessary to understand the influence of curing time and temperatures on the amount of binder present in the sample and the resulting bending strength and permeability of the 3DP mold.

The investigated 3D printed sand molds suffer from excessive moisture content generated from polycondensation reaction after printing and require subsequent ageing in order to remove excess water content affecting the 3PB strength. For this reason, oven curing at low temperatures is suggested primarily so as to remove excessive moisture content. Besides, as mentioned above, the strengthening mechanism consists in curing of the binder and its subsequent solidification leading to hardening of the resin bridges and cohesion between sand grains. For these reasons, curing time and temperature have a significant influence on the strength and permeability of the printed molds. Since the boiling points at room conditions of water and furfuryl alcohol are 100°C and 180°C respectively, different curing temperatures were chosen to investigate the ageing mechanisms: 25º C, 100°C and 200°C.

In the present work, the influence of the evaporation of each of the components on the 3PB strength and permeability of the 3DP mold were evaluated separately. The uncured condition corresponds to the initial stage of the 3DP before heating, after several hours self-curing at room temperature. The oven-cured stage corresponds to the post-processing of the 3DP by heating in an air-ventilated oven at 100°C and 200°C for several hours. The samples were removed from the oven and were allowed to cool down to room temperature before each test.

The specimens were weighed every 12 h up to 60 h during storage at each curing temperature in order to assess the effect of mass loss rate during ageing. The length, the breadth and the height of the 3D printed bars were controlled every 2 h to 60 h during storage at each curing temperature in order to monitor the dimensional variations of the sand samples over time. No significant change was observed. Then, 3PB test and gas permeability tests were conducted at curing times ranging from 0 to 60 h. Here 0 h represent the time when the specimens were printed. An interval of 2 hours was chosen in between measurements for the first 60 hours. After that, the specimens were tested once after every 7 days, and continued up to 54 days. The selected storage times were relevant for high-volume mold production and storage for a longer time at industrial scale. In particular, the initial strength of the 3D printed sand cores is important for manipulation of the mold after printing, and was tested 5 minutes after production. The results after 2 and 60 h were representative of the 3D printed mold/core properties at the beginning and end of a typical core usage in foundry practice, and the results from 60 h to 54 days were representative of the 3D printed mold/core properties during storage.

Density and porosity

The porosity of the samples was determined with the oven-dry method [46]. The particle density was considered as being the density of SiO_2-quartz (2648 $kg.m^{-3}$), which constitutes 99.1% of the sand used by the printer. A laboratory precision balance was used to weight the printed specimens after drying in a hot-air oven at 105°C for 24 hours, and the bulk density of the 3DP specimen was calculated as the mass of sample per unit bulk volume. It is worth reminding that both the volume of solid and the volume of pores were taken into account for the calculation of bulk density. In contrast, the particle density was equal to the mass of sample per unit volume of silica sand particles.

From the bulk density and particle density, the total porosity of the 3DP specimens was calculated as, $\text{Porosity}(\%) = (1 - (\text{Bulk density})/(\text{Particle density})) \times 100.$

The experimentally measured porosity values were close to 49% for all tested samples, with an estimated standard deviation of 0.2%. This porosity value roughly corresponds to the theoretical porosity of a simple cubic packing (~48%).

Loss on Ignition

Loss on Ignition is a widely used procedure to measure the amount of moisture, binder and impurities present in the sample through ignition at high temperatures. Three 3DP specimens were printed for this test, and the weight was close to 30g (initial mass) in all cases in agreement with previous works [26]. These specimens were then put into the ceramic crucibles. Before filling, the crucibles were pre-heated at 100°C in an oven to extract moisture and organic residues. After that, the 3DP specimens were put inside the crucibles and heated at 900°C for 30mins to burn-out and expel the binder and moisture. Then, the crucible was removed from the oven, and weight of the crucible was measured. The final mass is the weight of the burnt out specimen. LOI was then determined from Eq. (4):

$$LOI = \frac{Initial\ mass - Final\ mass}{Initial\ mass} \times 100 \quad \% \tag{4}$$

Images of the crucibles containing the tested samples at the different stages of the LOI tests are provided in Fig.4. An average mass loss of 1.41%, with an estimated standard deviation of 0.02%, was measured by the LOI tests performed on the sand mold samples. The low variability observed in the measured mass loss values of the tested samples was an indicator of the high reproducibility of the binder dosage process.

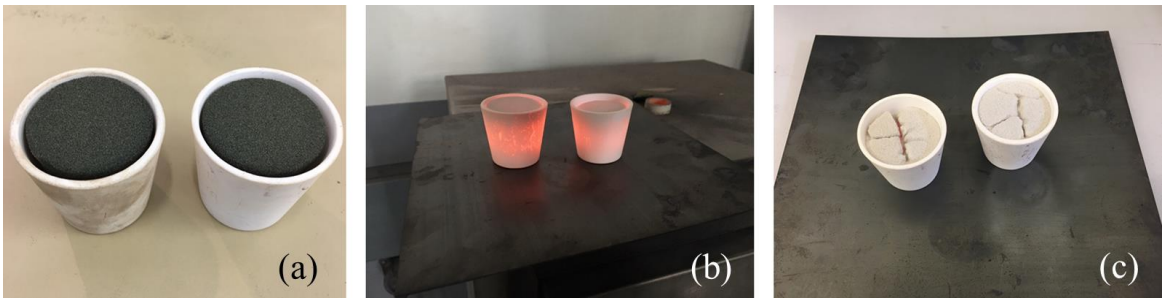

Fig.4 LOI test crucible with (a) powdered 3DP specimens,(b) immediately after taking out of the oven at 900 °C and (c) after cooling it to 150 °C, before weighting the final mass

Three-point Bending test

The bending strength of the 3DP specimens was determined using a 3PB test, which is a destructive method commonly used for testing traditionally prepared sand molds. To determine the 3PB strength of the 3DP specimens, bars with a square section of length b = 172 mm, and width d = 22.4 mm were printed. 3PB tests were performed on the 3DP bar specimens using a Simpson-Electrical PFG type universal strength test machine [47, 48], shown in Fig.5. This universal strength machine is widely used to measure the strength of resin bonded sand molds. The test fixture constitutes of two supporting pins, with a separation distance of l =150 mm. The load applied by the third pin was progressively increased at a rate of 0.1 MPa.s^{-1} until the samples broke and the 3PB strength was determined by reading the pressure gauge. The measuring range of the machine covered up to 12.8 MPa, with an reading uncertainty on the pressure gauge of ±0.05 MPa.

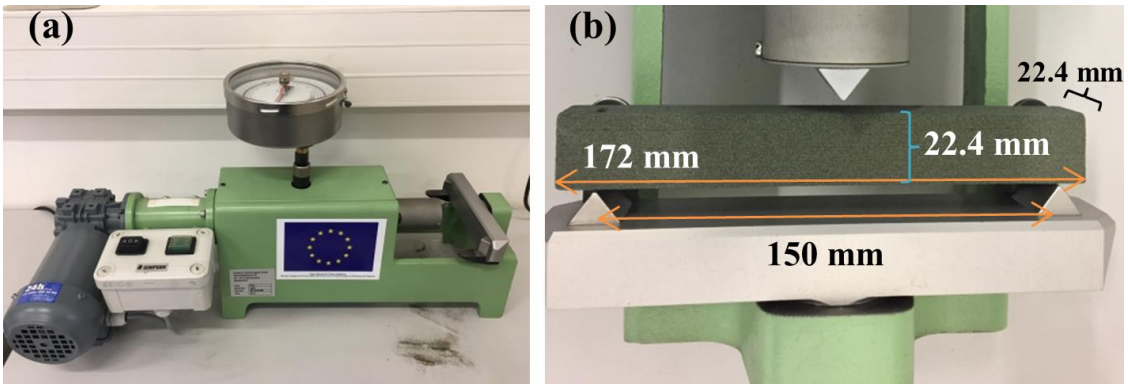

Fig.5 Universal strength machine used for the 3PB test [48], (a) front view and (b) dimensions of the bar

Gas permeability test

A permeability measurement device Simpson-Electrical, Type: PFG, Serial No.3290, Item No.592-824-600, [49] was used in the present experiments to measure the gas permeability of the 3DP sand mold samples following the recommendations of the American Foundry Society (AFS). The gas permeability value (GP) gives the volume of air in cm^3 which passes through a cylinder, having a cross-sectional area of $1cm^2$ and a height of 1 cm, in 1 minute at a

pressure of 100 mm SPWG (Static Pressure Water Gauge). The relationship for the calculation of GP is expressed by the following formula:

$$GP = \frac{V \times h}{F \times p \times t} \quad (5)$$

where, V is the volume of air flowing through the tested sample, h is the height of the sample , F is the cross-sectional area of the sample, p is the pressure in mm Static Pressure Water Gauge (SPWG) and t is the passage time for 2000 cm^3 of air in minutes. In the present tests, the values V = 2000 cm^3, h = 5 cm, F = 19.63 cm^2 and p = 100 mm SPWG = 980 Pa were used [49–51] and the resulting t was measured. The viscosity of the fluid (air) was taken as 1.8×10^{-5} Pa sec. Cylindrical samples with a diameter of d = 50 mm and length of l = 50 mm were used in these tests. The flow rate was measured with the digital permeability meter (Simpson-Digital permeability meter) [49], which has a measuring range of 0-1000 GP. It should be noted that Eq. (5) does not provide k as defined by Eq. (1). Indeed, GP obtained from Eq. (5) is gas viscosity-dependent while k obtained from Eq. (1) does not depend on the physical properties of the injected fluid. However, GP is commonly used in foundry industries as recommended by the American foundry society (AFS). For this reason, the results of permeability measurements will be presented in terms of GP in this work.

IV. RESULTS

The ageing effect on weight loss, 3PB strength and permeability were experimentally investigated using the tests presented in the preceding section.

The results in terms of mass loss as a function of curing time are presented in Fig.6. It can be noted that, as expected, the total weight loss after curing was lower for 25°C and 100°C° than it was for 200°C. It was also observed that the evaporation rate increased with increasing curing times at 200°C. The amount of weight loss at 200°C was higher after 36 hours, due to

the evaporation of both alcohol and water. Although the 3PB test were performed for all the specimens heat treated at 200°C, but it was not possible to measure the weight loss accurately after 36 hours due to loss of little sand particle while handling.

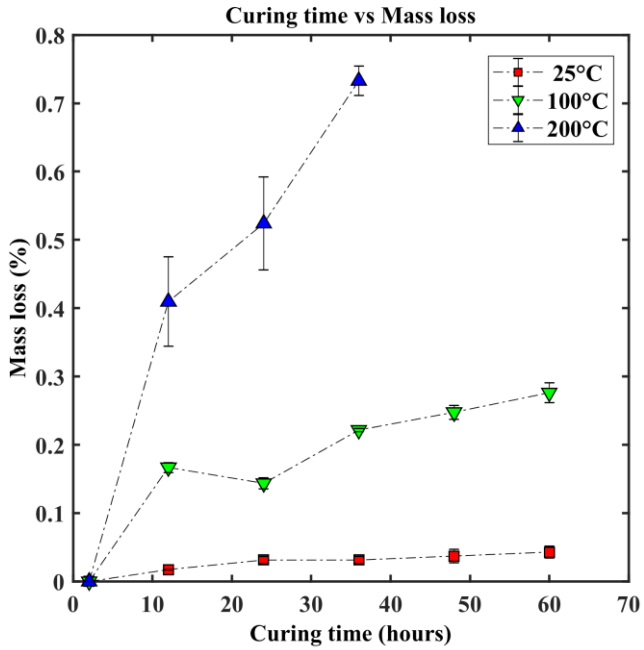

Fig.6 Critical effect of curing time and temperature on mass loss of specimens

The length, the breadth and the height of the 3D printed bars were controlled every 2 h to 60 h during storage at each curing temperature in order to monitor the dimensional variations of the sand samples over time. No significant change was observed. The 3PB strength of the samples is presented in Fig.7 as a function of the curing time for the three curing temperatures. From this figure, it can be deduced that bending strength remains approximately constant over time in the case of curing at 25ºC and 100ºC, apart from an initial increase in strength. However, a different tendency was observed when curing at 200ºC. Indeed, the bending strength decreased over time, roughly monotonically, for this curing temperature. Moreover, the values of 3PB obtained by ageing at 25ºC and 100ºC were very close and significantly greater than those obtained by ageing at 200ºC. It was noted that the measurements at 200ºC did not cover the full range of times up to 1296 h as the bending strengths were too low and did not fall within the working range of the apparatus for the further measurements.

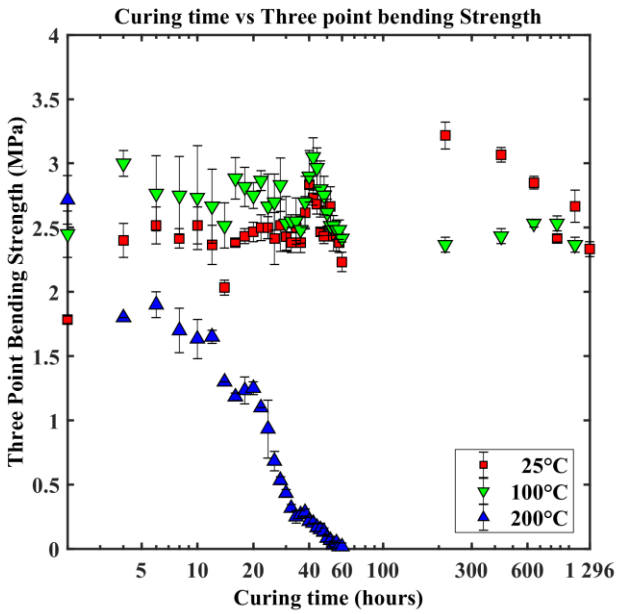

Fig.7 Critical effect of curing time and temperature on 3PB strength of specimens

The permeability values of the mold samples measured at different curing times are presented in Fig.8 for the three investigated curing temperatures. From this figure, the results showed that permeability remained approximately constant over time in the case of curing at 25ºC and 100ºC. However, a decrease in permeability over time was remarked when curing at 200ºC. Also, the permeability was shown to decrease with curing temperature, and the reasons will be discussed in section 5.

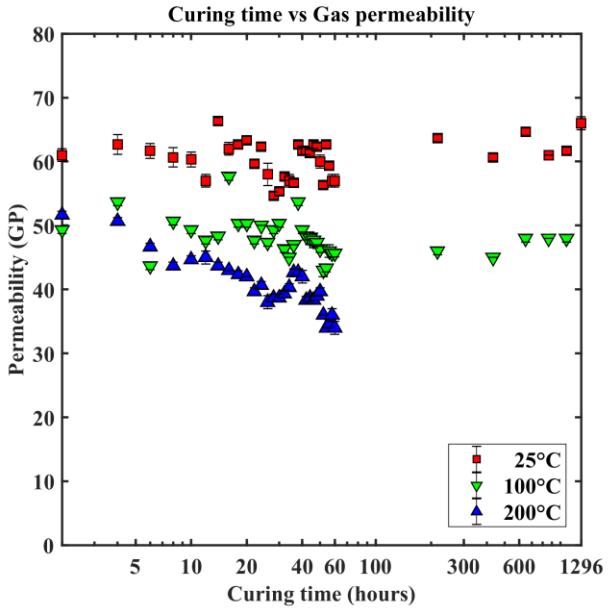

Fig.8 Permeability of the samples vs. curing time at different temperatures

The results in terms of mass loss as a function of 3PB strength and permeability were presented in Fig.9and 10. The mass loss at low temperatures may be explained by rapid evaporation of solvent. Moreover, a second stage occurs at high temperature when the resin bridge becomes brittle and breaks for prolonged heating at high temperatures, leading to loosening of powdered particles. Fig.9 shows that the 3PB strength was higher at 100°C as compared to the samples at 25°C, but decreased gradually at 200°C. However, permeability decreased with increased mass loss as can be observed in Fig.10. This is in contrast with the results obtained by previous researchers [20] and will be discussed in the following section.

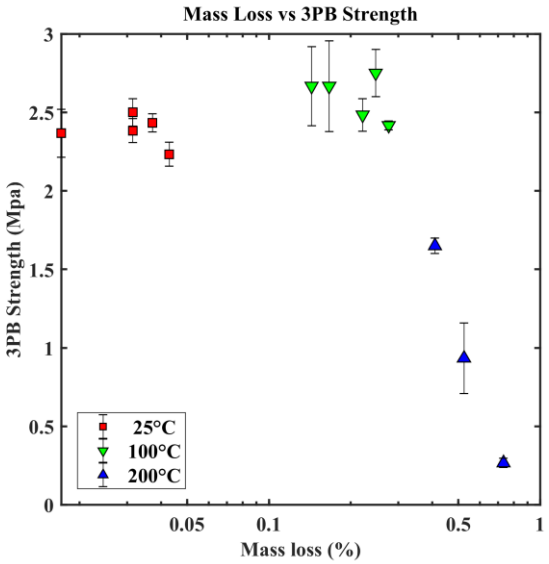

Fig.9 3PB strength vs. mass loss for the three curing temperatures

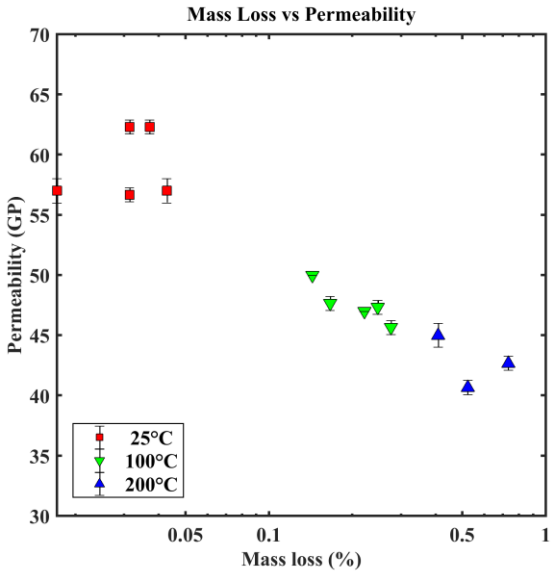

Fig.10 Permeability vs. mass loss for the three curing temperatures

V. DISCUSSION

The solvent present in the binder is volatile and evaporates during the ageing process, leading to shortening and hardening of the resin bridges. Only water experiences significant evaporation with time at 25º C. Also, water evaporates faster at 100°C than it does at 25º C (the boiling temperature of water is close to 100°C under the experimental conditions of our tests), which results in higher values of mass loss as reported in Fig.6. On the other hand, the boiling temperature of furfuryl alcohol is 180°C, so it is the mixture of water and alcohol which experiences significant evaporation when curing at 200°C. The higher rate of evaporation at 200ºC leads to higher values of weight loss as shown in Fig.6. The increase of evaporation rate with increasing curing time reported at 200ºC may be related to the increase in the area of the free surface of liquid (binder + water) with time. Indeed, the specific surface area of the liquid is expected to increase as it progressively evaporates, resulting in higher evaporation rates.

It was observed in Fig.7 that the 3PB strength experienced an initial increase before becoming constant with time after ~ 4h for 25ºC and 100ºC. This effect is generally associated with water being released during polycondensation occurring at the initial stages of curing, which leads to cross linked polymerization stemming from exothermic polycondensation [24]. This hardens the resin bridges between sand grains, providing greater mechanical strength (3PB) to the 3DP specimen. Moreover, the polymer chain network is expected to break gradually at 200°C as the alcohol evaporates. This results in lower 3PB strength, of the 3DP specimens as presented in Fig.7, in good agreement with the results of previous researchers [20].

In the case of the present experiments, the furan system is a thermosetting resin (duroplast) which forms an insoluble infusible 3-dimensional polymer network chain through polymerization during curing stage [24]. The gradual increase in strength at lower temperatures (25°C, 100°C) may be related to the evaporation of the solvent, which causes shortening and hardening of resin bridges. This leads to both a gradual increase in 3PB strength and shrinkage of the mold [22]. The shrinkage of the mold samples during curing was also reported in previous works [22, 27, 52]. Therefore, an increase in ageing time causes more volumetric reduction of furan resin bridges, which results in more shrinkage and

reduction of pore space between sand grains [11, 22], thus leading to lower gas permeability values. This is consistent with the results presented in Fig.10.

The FNB is injected between the sand particles, filling the interstices and reducing the effective pore size available for gas flow. This presence of binder layers that settle on the grain walls results in permeability reduction as predicted by Eq. (2). Consequently, as the binder evaporates, the effective pore size should increase leading to higher permeability values. However, shrinkage occurs simultaneously, so the sand particles should also become more tightly packed as they are dragged by the remaining binder. As a result, the variation in permeability during binder evaporation is expected to be the combination of both effects. Given that Loss On Ignition is low (1.41%), the volume fraction of the pores occupied by binder should be also low. Therefore, shrinkage is expected to be the dominant mechanism which explains the reduction in permeability.

Using Eq. (2), a permeability of 4.9×10^{-11} m^2 (or) 49 Darcy is predicted for a sand packing with porosity 0.49 and grain size of 140μm, which is close to the measured value $k = 5.57 \times 10^{-11}$ m^2 (or) 56 Darcy provided by Eq. (1) for the present experiments. The slight difference between prediction and experiments may be explained by the presence of binder within the pores, which increases the effective d_s in Eq. (2). Indeed, if the experimentally measured value of permeability value (k=56 Darcy) is used in Eq. (2), an effective grain diameter of ~ 155 μm is obtained. It is reminded that Eq. (2) provides accurate predictions in the case in which the volume fraction of binder (determined by LOI tests) is low.

The GP values obtained with the current technique are viscosity-dependent as can be deduced from comparison between Eqs. (1) and (5). However, gas viscosity increases with temperature, thus generating greater pressure losses for the same flow rate at higher temperatures. Neither are other effects such as inertial pressure losses, fluid's compressibility or slip on the wall taken into account by the permeability tests currently used in casting industry. Therefore, a new approach should be developed to obtain more accurate permeability values, which should improve the prediction of casting defects. Also, the three-point bending test can only be used for measuring the strength in a particular region of the

3DP specimen, so a different approach should be used to characterize the global strength of the samples.

VI. CONCLUSIONS

The effects of curing time and temperature on the permeability and 3PB strength of 3DP sand mold samples were experimentally evaluated. Both permeability and 3PB strength were shown to be altered by the curing process under certain conditions. Hardening of the binder and shrinkage of the mold arising from polycondensation reaction of the binder, which is a cross-linked, high-strength thermoset, may explain this. The following industrial implications are drawn:

- ✓ The printed molds can be stored at room temperature for a long time before being used, roughly preserving the initial values of 3PB strength and permeability.

- ✓ From the bulk density and the particle density values of the 3DP mold, the sand grains can be packed in a simple cubic structure, obtaining a porosity of 48%.

- ✓ Despite not taking into account the volume of binder in the pores, the prediction provided by Kozeny–Carman equation was in good agreement with experimental permeability measurements obtained with a standard permeameter. This is explained by a low fraction of the pore volume being occupied by the binder, as deduced from the LOI tests.

- ✓ The permeability of the 3D printed specimen decreases with increasing temperature, which is potentially due to shrinkage of the 3DP sand mold.

VII. ACKNOWLEDGEMENTS

The assistance during 3D printing of sand specimens by Mr. Jérémie Bourgeois and the collaboration with the LIST laboratory of CEA TECH, are greatly acknowledged.

REFERENCES

1. Sachs EM, Haggerty S, Michael J, Williams PA (1993) Three-Dimensional Printing Techniques. U.S. Pat. 5 340 656 1–15

2. Sachs E, Cima M, Cornie J, et al (1993) Three-Dimensional Printing: The Physics and Implications of Additive Manufacturing. CIRP Ann - Manuf Technol 42:257–260 . doi: 10.1016/S0007-8506(07)62438-X

3. Bredt JF, Anderson T (1999) Method of three dimensional printing. United States Pat.

4. Sachs E, Cima M, Cornie J, et al (1990) Dimensional Printing: Rapid Tooling and Prototypes Directly from CAD Representation. Solid Free Fabr Symp 27–47 . doi: 10.1016/S0007-8506(07)61035-X

5. Upadhyay M, Sivarupan T, El Mansori M (2017) 3D Printing for Rapid Sand Casting - A Review. J Manuf Process 29:211–220 . doi: 10.1016/j.jmapro.2017.07.017

6. Almaghariz ES (2015) Determining When to Use 3D Sand Printing : Quantifying the Role of Complexity By Eyad S . Almaghariz A thesis Submitted in Partial Fulfillment of the Requirements for the Degree of Master of Science in the

7. Almaghariz ES, Conner BP, Lenner L, et al (2016) Quantifying the role of part design complexity in using 3d sand printing for molds and cores. Int J Met 10:240–252 . doi: 10.1007/s40962-016-0027-5

8. Conner BP, Manogharan GP, Martof AN, et al (2014) Making sense of 3-D printing: Creating a map of additive manufacturing products and services. Addit Manuf 1:64–76 . doi: 10.1016/j.addma.2014.08.005

9. Low ZX, Chua YT, Ray BM, et al (2017) Perspective on 3D printing of separation membranes and comparison to related unconventional fabrication techniques. J Memb Sci 523:596–613 . doi: 10.1016/j.memsci.2016.10.006

10. Shepler J, Chapman S (2017) ExOne - A Case Study in Optimizing Casting Design Using 3 D Printing

11. Khandelwal H, Ravi B (2016) Effect of molding parameters on chemically bonded sand mold properties. J Manuf Process 22:127–133 . doi:

10.1016/j.jmapro.2016.03.007

12. Nastac L, Jia S, Nastac MN, Wood R (2016) Numerical modeling of the gas evolution in furan binder-silica sand mold castings. Int J Cast Met Res 29:194–201 . doi: 10.1080/13640461.2015.1125983

13. Tiedje N, Crepaz R, Eggert T, Bey N (2010) Emission of organic compounds from mould and core binders used for casting iron, aluminium and bronze in sand moulds. J Environ Sci Health A Tox Hazard Subst Environ Eng 45:1866–1876 . doi: 10.1080/10934529.2010.520595

14. Motoyama Y, Inoue Y, Saito G, Yoshida M (2013) A verification of the thermal stress analysis, including the furan sand mold, used to predict the thermal stress in castings. J Mater Process Technol 213:2270–2277 . doi: 10.1016/j.jmatprotec.2013.06.024

15. Marumoto N, Kashimura H, Yoshida K, et al (2016) Dynamic measurements of the load on gray cast iron castings and contraction of castings during cooling in furan sand molds. J Mater Process Technol 237:48–54 . doi: 10.1016/j.jmatprotec.2016.05.012

16. Sanitas A, Coniglio N, Bedel M, El Mansori M (2017) Investigating surface roughness of ZE41 magnesium alloy cast by low-pressure sand casting process. Int J Adv Manuf Technol 92:1883–1891 . doi: 10.1007/s00170-017-0283-4

17. Bobby SS (2014) A Preliminary Investigation of Gypsum Bonded Moulds By Three Dimensional Printing. IJRET Int J Res Eng Technol 3:501–507

18. Frascati J (2007) Effects of Position, Orientation, and Infiltrating Material on Three Dimensional Printing Models. Dep Mech Mater Aerosp Eng degree of: . doi: 10.1017/CBO9781107415324.004

19. Vaezi M, Chua CK (2011) Effects of layer thickness and binder saturation level parameters on 3D printing process. Int J Adv Manuf Technol 53:275–284 . doi: 10.1007/s00170-010-2821-1

20. Mckenna N, Singamneni S, Diegel O, et al (2008) Direct Metal casting through 3D printing : A critical analysis of the mould characteristics. 9th Glob Congr Manuf Manag 12–14

21. Snelling D, Williams CB, Druschitz AP (2014) A Comparison of Binder Burnout and

Mechanical Characteristics of Printed and Chemically Bonded Sand Molds. SFF Symp 197–209

22. Khandelwal H, Ravi B (2015) Effect of Binder Composition on the Shrinkage of Chemically Bonded Sand Cores. Mater Manuf Process 30:1465–1470 . doi: 10.1080/10426914.2014.994779

23. Meisel N a., Williams CB, Druschitz A (2012) Lightweight Metal Cellular Structures via Indirect 3D Printing and Casting. Solid Free Fabr Symp 162–176

24. Renhe H, Hongmei G, Yaoji T, Qingyun L (2011) Curing mechanism of furan resin modified with different agents and their thermal strength. China Foundry 8:161–165

25. Gill SS, Kaplas M (2011) Efficacy of powder-based three-dimensional printing (3DP) technologies for rapid casting of light alloys. Int J Adv Manuf Technol 52:53–64 . doi: 10.1007/s00170-010-2716-1

26. Günther D, Mögele F (2016) Additive Manufacturing of Casting Tools Using Powder-Binder- Jetting Technology. In: New Trends in 3D Printing. InTech

27. Bobrowski A, Grabowska B (2012) The impact of temperature on furan resin and binder structure. Metall Foundry Eng 38:73–80

28. Zeitsch KJJ (2001) The Chemistry and Technology of Furfural and its Many By Products

29. Quaker T, Company O (1984) Catalyst composition and method for curing furan-based foundry binders-US 4451577 A

30. Bassoli E, Atzeni E (2009) Direct metal rapid casting: mechanical optimization and tolerance calculation. Rapid Prototyp J 15:238–243 . doi: 10.1108/13552540910979758

31. Darcy HPG (1856) Les fontaines publiques de la ville de Dijon. Libraire des Corps imperiaux des ponts et chaussées et des mines, Paris

32. Gardziella A, Pilato LA, Knop A (2013) Phenolic resins: chemistry, applications, standardization, safety and ecology. Springer Science & Business Media.

33. ExOne (2017) ExOne: Digital Part Materialization

34. ExOne (2013) FS001 (Silica sand)-Material data sheet. 1:2013

35. ExOne (2014) FB001 (Furan Binder) - Fiche De Données De Sécurité Caprolactam,selon 1907/2006/CE, Article 31. 2–11

36. Holtzer M, Dańko R (2015) Molds and Cores Systems in Foundry. 27–43 . doi: 10.1007/978-3-319-14583-9

37. Dassault Systèmes (2017) Catia V5

38. Autodesk Inc (2017) Netfabb®

39. ExOne (2014) S-Print ™ Furan

40. Sivarupan T, ElMansori M, Coniglio N (2017) 3D Printing Process Parameters and Properties of Additively Manufactured Sand Mold for Rapid Casting : Strength and Permeability. Addit Manuf (under review)

41. Coniglio N, Sivarupan T, El Mansori M (2017) Investigation of process parameter effect on anisotropic properties of 3D printed sand molds. Int. J. Adv. Manuf. Technol. 1–11

42. Lee JJ, Sachs E, Cima M (1995) Layer position accuracy in powder based rapid prototyping. Rapid Prototyp J 1:24–37 . doi: 10.1108/13552549510104447

43. Dimitrov D, Beer N (2006) Developing capability profile for the three dimensional printing process. R D J 22:17–25

44. D.M. Dimitrov, N. de Beer (2014) IMPROVEMENTS IN THE CAPABILITY PROFILE OF 3-D PRINTING: AN UPDATE. South African J Ind Eng 25:1–12 . doi: 10.11842/wst.2014.02.015

45. Hościło B, Kaczyński R, Skorulski G (2014) Rapid Prototyping Technology Using for Casting Process of Mini Turbine Runner. Arch Foundry Eng 14:83–86

46. C. O. Willits's (1951) Methods for Determination of Moisture-Oven Drying. Anal Chem 1058–1062 . doi: 10.1021/ac60056a003

47. Simpson Technologies Corporation (2008) SIMPSON Sand Testing machines for Molding and Core Sands DESIGNED

48. Simpson (2008) SIMPSON Universal Strength Machine PFG

49. Simpson (2002) Simpson Permeability Meter PDU-D

50. DISA Industrie AG (2017) Testing instruments and accessories to determine the permeability of moulding and core sands

51. Georges Fischer société anonyme (2017) Permeametre type PDU

52. Lowe K E, Showman R E (2011) Dimensional Changes in Chemically Bonded Molds and Cores. Trans Am Foundry Soc 119:251–260